Int J Fract (2007) 145:341–347
DOI 10.1007/s10704-007-9137-7

LETTERS IN FRACTURE AND MICROMECHANICS

ON EFFECTIVE ENERGY REFLECTANCE OF PARTICULATE MATERIALS

F. Dirksen and T. I. Zohdi
Department of Mechanical Engineering
6195 Etcheverry Hall
University of California, Berkeley, CA, 94720-1740, USA
email: frank_dirksen@berkeley.edu, zohdi@newton.berkeley.edu (corresponding author)

Abstract. This paper investigates the effective energy reflectance of materials comprised of a continuous matrix embedded with fine-scale particles of different electric permittivity and magnetic permeability. The specific objective is to determine under what conditions will increasing the particulate volume fraction initially increase (or decrease) the overall reflectance from a pure-matrix base state and, with further increase in volume fraction, *reverse* the trend, i.e. decrease (or increase) the effective reflectance. The importance of this condition is that it indicates when the correlation of a specific level of reflectance to a specific volume fraction of particles may not be unique, even when the properties of the particles and matrix are fixed.

Keywords: particulate media, effective reflectance

1 Introduction. There is a large number of materials comprised of a continuous matrix with embedded particles, such as composites and, clearly, paints and coatings, where the overall electromagnetic, in particular optical, reflectance is important. In fluid mechanics, noninvasive monitoring techniques, such as laser or infrared velocemitry, for particle-laden flow processes are now playing an increasingly central role in experiments. For example, in Chung et al. (1999) techniques for measuring flow characteristics based upon Infrared Thermal Velocimetry (ITV) in fluidic microelectromechanical systems (MEMS) have been developed where infrared lasers are used to generate a short energy (heating) pulse in a flowing liquid, and an infrared camera records the subsequent radiative emission. The flow properties are obtained from consecutive radiative energy images. Such techniques are directly applicable to complex particle-laden flows. Furthermore, for particle-laden bio-fluid flow, similar techniques, based on optical energy reflectance, are widely used to determine aggregate blood flow properties in the analysis of heart disease (Chau et. al (2004), Khalil et. al (2005), Chan et. al (2004) and Bale-Glickman et al. (2003 a, b)). Such techniques can be used to monitor cutting-edge industrial processes such as Chemical Mechanical Planarization (CMP), which involve employing fine-scale chemically-reacting particles embedded within a fluid (gas or liquid) to ablate small-scale rough surfaces flat. For reviews of CMP practice and applications, see Luo and Dornfeld (2001, 2003a, 2003b, 2004). Finally, in atmospheric and astrophysical studies concerned with the behavior of dust, much of the collected data is based on some type of electromagnetic, typically optical, measurement. For reviews of astrophysical dust-related phenomena, see Benz (1994, 2000), Blum and Wurm (2000), Dominik and Tielens (1997), Chokshi et al. (1993), Wurm et al. (2001), Cuzzi et al. (1993) and Beckwith et al. (2000). In all

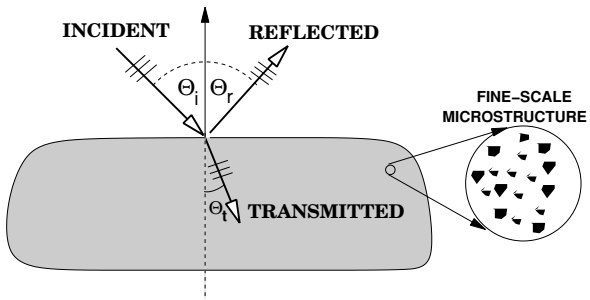

Figure 1: Nomenclature for a reflection.

of the mentioned applications, the overall reflectance of the particulate system is an important quantity to ascertain. For more applications, see Zohdi (2004, 2006a, b, c, 2007).

The focus of this work is to investigate the dependence of the overall electromagnetic energy reflectance of heterogeneous materials, comprised of a continuous matrix with embedded randomly dispersed particles (Figure 1), on the particulate volume fraction. *Throughout this work we consider cases where the wavelength of the electromagnetic fields is much larger than the length-scales associated with the microstructure.*

2 Maxwell's Equations. The free space propagation of electromagnetic waves can be described by a simplified form of Maxwell's equations

$$\nabla \times \boldsymbol{E} = -\mu_o \frac{\partial \boldsymbol{H}}{\partial t} \qquad \text{and} \qquad \nabla \times \boldsymbol{H} = \epsilon_o \frac{\partial \boldsymbol{E}}{\partial t}, \tag{1}$$

with $\nabla \cdot \boldsymbol{H} = 0$ and $\nabla \cdot \boldsymbol{E} = 0$, where $\boldsymbol{E}$ is the electric field intensity, $\boldsymbol{H}$ is the magnetic flux intensity, ϵ_o is the permittivity and μ_o is the permeability in vacuum (denoted by index 0). Using standard vector identities, one can show that

$$\nabla \times (\nabla \times \boldsymbol{E}) = -\mu_o \epsilon_o \frac{\partial^2 \boldsymbol{E}}{\partial t^2} \qquad \text{and} \qquad \nabla \times (\nabla \times \boldsymbol{H}) = -\mu_o \epsilon_o \frac{\partial^2 \boldsymbol{H}}{\partial t^2}, \tag{2}$$

and consequently

$$\nabla^2 \boldsymbol{E} = \tfrac{1}{c^2} \frac{\partial^2 \boldsymbol{E}}{\partial t^2}, \qquad \text{and} \qquad \nabla^2 \boldsymbol{H} = \tfrac{1}{c^2} \frac{\partial^2 \boldsymbol{H}}{\partial t^2}, \tag{3}$$

where the speed of electromagnetic wave propagation is $c = \frac{1}{\sqrt{\epsilon_o \mu_o}} \approx 2.997924562 \times 10^8 \pm 1.1\, m/s$ in vacuum. The free space electric permittivity is $\epsilon_o = \frac{1}{c^2 \mu_o} = 8.8542 \times 10^{-12}\ CN^{-1}m^{-1}$ and the free space magnetic permeability is $\mu_o = 4\pi \times 10^{-7}\ WbA^{-1}m^{-1} = 1.2566 \times 10^{-6}\ WbA^{-1}m^{-1}$.

Now consider the special case of plane harmonic waves, for example of the form

$$\boldsymbol{E} = \boldsymbol{E}_o cos(\boldsymbol{k} \cdot \boldsymbol{r} - \omega t) \qquad \text{and} \qquad \boldsymbol{H} = \boldsymbol{H}_o cos(\boldsymbol{k} \cdot \boldsymbol{r} - \omega t), \tag{4}$$

where $\boldsymbol{r}$ is an initial position vector to the wave front, where $\boldsymbol{k}$ is the direction of propagation. For plane waves, $\boldsymbol{k} \cdot \boldsymbol{r} = constant$. We refer to the phase as $\phi =$

$\boldsymbol{k}\cdot\boldsymbol{r}-\omega t$, and $\omega=\frac{2\pi}{\tau}$ as the angular frequency, where τ is the period. For plane waves, the wave front is a plane on which ϕ is constant, which is orthogonal to the direction of propagation, characterized by $\boldsymbol{k}$. In the case of harmonic waves, we have $\boldsymbol{k}\times\boldsymbol{E}=\mu_o\omega\boldsymbol{H}$, $\boldsymbol{k}\times\boldsymbol{H}=-\epsilon_o\omega\boldsymbol{E}$ and $\boldsymbol{k}\cdot\boldsymbol{E}=0$ and $\boldsymbol{k}\cdot\boldsymbol{H}=0$. The three vectors, $\boldsymbol{k}$, $\boldsymbol{E}$ and $\boldsymbol{H}$ constitute a mutually orthogonal triad. By combining the previous relations one obtains $||\boldsymbol{k}||=\frac{\omega}{c}$. The direction of wave propagation is given by $\frac{\boldsymbol{E}\times\boldsymbol{H}}{||\boldsymbol{E}\times\boldsymbol{H}||}$.

3. Energy propagation. Electromagnetic waves travelling through space carry energy which flows in the direction of wave propagation. The energy per unit area per unit time flowing perperdicularly into a surface in free space is given by the Poynting vector $\boldsymbol{S}=\boldsymbol{E}\times\boldsymbol{H}$. For many types of electromagnetic energy, the frequencies of $\boldsymbol{E}$, $\boldsymbol{H}$ and $\boldsymbol{S}$ oscillate rapidly, and it is impractical to measure instantaneous values of $\boldsymbol{S}$ directly. Therefore, some type of time-averaging is performed. For example, consider the harmonic representations in Equation 4 which leads to $\boldsymbol{S}=\boldsymbol{E}_o\times\boldsymbol{H}_o cos^2(\boldsymbol{k}\cdot\boldsymbol{r}-\omega t)$, and consequently the average value over a longer time interval than the time scale of rapid random oscillation,

$$\langle\boldsymbol{S}\rangle_{\mathcal{T}}=\boldsymbol{E}_o\times\boldsymbol{H}_o\langle cos^2(\boldsymbol{k}\cdot\boldsymbol{r}-\omega t)\rangle_{\mathcal{T}}=\tfrac{1}{2}\boldsymbol{E}_o\times\boldsymbol{H}_o, \tag{5}$$

which consequently leads to the irradiance

$$I\overset{\text{def}}{=}||\langle\boldsymbol{S}\rangle_{\mathcal{T}}||=\tfrac{1}{2}||\boldsymbol{E}_o\times\boldsymbol{H}_o||=\tfrac{1}{2}\sqrt{\tfrac{\epsilon_o}{\mu_o}}||\boldsymbol{E}_o||^2. \tag{6}$$

Thus, the rate of flow of energy is proportional to the square of the amplitude of the electric field. Furthermore, in isotropic media, which we consider for the remainder of the work, the direction of energy is in the direction of $\boldsymbol{S}$ and in the same direction as $\boldsymbol{k}$.

4. Reflection and absorption of energy. Referring to Figure 1, when a wave encounters a material interface, the angle of incidence between the propagation direction and the outward unit surface normal (θ_i) lay in the same plane, with the reflected angle being equal to the indecent one ($\theta_r=\theta_i$). The angle of the transmitted wave's propagation direction (θ_t) is given by $n\overset{\text{def}}{=}\frac{c}{v}=\frac{sin\theta_i}{sin\theta_t}$, where c is the propagation speed in a vacuum and v is the propagation speed in the incident medium. When we consider a plane harmonic wave The amount of incident electromagnetic energy (I_i) that is reflected (I_r) is given by the total reflectance ($0\le R\le 1$)

$$R\overset{\text{def}}{=}\underbrace{\frac{I_r}{I_i}}_{\text{generally}}=\underbrace{\frac{1}{2}\left(\left(\frac{\frac{\hat{n}^2}{\hat{\mu}}cos\theta_i-(\hat{n}^2-sin^2\theta_i)^{\frac{1}{2}}}{\frac{\hat{n}^2}{\hat{\mu}}cos\theta_i+(\hat{n}^2-sin^2\theta_i)^{\frac{1}{2}}}\right)^2+\left(\frac{cos\theta_i-\frac{1}{\hat{\mu}}(\hat{n}^2-sin^2\theta_i)^{\frac{1}{2}}}{cos\theta_i+\frac{1}{\hat{\mu}}(\hat{n}^2-sin^2\theta_i)^{\frac{1}{2}}}\right)^2\right)}_{\text{unpolarized waves}}, \tag{7}$$

where $\hat{n}$ is the ratio of the refractive indices of the ambient (incident) medium (n_i) and transmitted particulate medium (n_t), $\hat{n}=n_t/n_i$, $\hat{\mu}$ is the ratio of the magnetic

permeabilities of the surrounding incident medium (μ_i) and transmitted particulate medium (μ_t), $\hat{\mu} = \mu_t/\mu_i$. Specifically, if the wave is directly incident ($\theta_i = 0$),

$$R \stackrel{\text{def}}{=} \frac{I_r}{I_i} = \left(\frac{\hat{n}-\hat{\mu}}{\hat{n}+\hat{\mu}}\right)^2 = \left(\frac{\sqrt{\epsilon_t/\epsilon_i}-\sqrt{\mu_t/\mu_i}}{\sqrt{\epsilon_t/\epsilon_i}+\sqrt{\mu_t/\mu_i}}\right)^2 = \left(\frac{\sqrt{\hat{\epsilon}}-\sqrt{\hat{\mu}}}{\sqrt{\hat{\epsilon}}+\sqrt{\hat{\mu}}}\right)^2 \tag{8}$$

where $\hat{\epsilon} = \frac{\epsilon_t}{\epsilon_i}$ and $\hat{n} = \frac{n_t}{n_i} = \sqrt{\frac{\epsilon_t \mu_t}{\epsilon_i \mu_i}}$.

Remark: Equation 7, is a special case of the well-known Fresnel relations, and can be derived by considering a plane harmonic wave incident upon a plane boundary separating two different materials, which produces a reflected wave and a transmitted (refracted) wave (Figure 1). The usual approach is to consider two cases: (1) electric field vectors that are parallel to the plane of incidence and (2) electric field vectors that are perpendicular to the plane of incidence. In either case, the tangential components of the electric and magnetic fields are required to be continuous across the interface. This leads to the result in Equation 7. For more details see, for example, Born and Wolf (2003).

5. Overall properties. The isotropic effective property relations between displacement and electric field, for a heterogeneous medium, are described by $\langle \boldsymbol{B} \rangle_\Omega = \mu^* \langle \boldsymbol{H} \rangle_\Omega$ and $\langle \boldsymbol{D} \rangle_\Omega = \epsilon^* \langle \boldsymbol{E} \rangle_\Omega$, where $\langle (\cdot) \rangle_\Omega \stackrel{\text{def}}{=} \frac{1}{|\Omega|} \int_\Omega (\cdot)\, d\Omega$, where $\langle \boldsymbol{E} \rangle_\Omega$ is the overall electric field intensity, $\langle \boldsymbol{B} \rangle_\Omega$ is the overall magnetic flux density, $\langle \boldsymbol{H} \rangle_\Omega$ is the overall magnetic flux intensity, $\langle \boldsymbol{D} \rangle_\Omega$ is the overall electric displacement, μ^* is the effective magnetic permeability and ϵ^* is the effective permittivity. The effective reflectance defined as

$$R^* \stackrel{\text{def}}{=} \left(\frac{\sqrt{\hat{\epsilon}*}-\sqrt{\hat{\mu}^*}}{\sqrt{\hat{\epsilon}^*}+\sqrt{\hat{\mu}^*}}\right)^2 \tag{9}$$

where the *relative* effective values are $\hat{\epsilon}^* = \epsilon^*/\epsilon_i$, $\hat{\mu}^* = \mu^*/\mu_i$. *The effective permittivity ϵ^* and permeability μ^* depend on the volume fraction of the particulates (v_p) as well as the properties of the matrix and particle phases.*

6. Conditions for nonmonotone reflectance dependence on particulate volume fraction. A key effect which we wish to investigate is the nonmonotone dependence of the overall reflectance on the volume fraction of particles (v_p). Specifically, our interest is to determine under what conditions would increasing v_p initially increase (or decrease) R^* from a purely matrix material, then, with increase in v_p, *reverse* the trend, i.e. decrease (or increase) R^*. The point of change, i.e. the onset of this nonmonotone behavior occurs when the derivative of R^* with respect to v_p vanishes. In order to determine when this may occur we differentiate the overall reflectance with respect to the particulate volume fraction by first writing

$$dR^* = \frac{\partial R^*}{\partial \hat{\epsilon}^*} d\hat{\epsilon}^* + \frac{\partial R^*}{\partial \hat{\mu}^*} d\hat{\mu}^*, \tag{10}$$

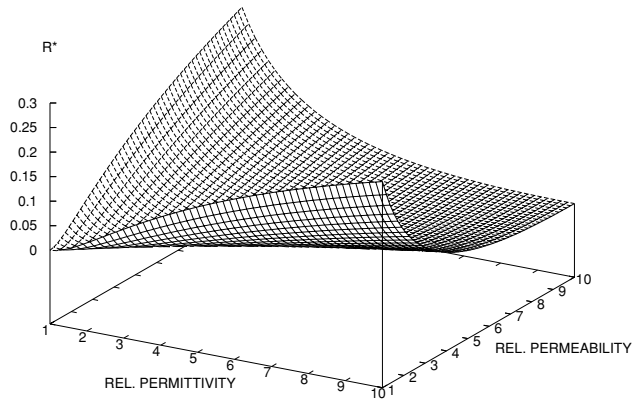

Figure 2: The behavior of R^* as a function of $\hat{\epsilon}^*$ and $\hat{\mu}^*$.

and expanding $d\hat{\epsilon}^* = \frac{\partial \hat{\epsilon}^*}{\partial v_p} dv_p$ and $d\hat{\mu}^* = \frac{\partial \hat{\mu}^*}{\partial v_p} dv_p$, we obtain

$$\frac{dR^*}{dv_p} = \frac{\partial R^*}{\partial \hat{\epsilon}^*} \frac{\partial \hat{\epsilon}^*}{\partial v_p} + \frac{\partial R^*}{\partial \hat{\mu}^*} \frac{\partial \hat{\mu}^*}{\partial v_p}. \tag{11}$$

One can show that

$$\frac{\partial R^*}{\partial \hat{\epsilon}^*} = 2 \frac{\sqrt{\hat{\mu}^*}}{\sqrt{\hat{\epsilon}^*}} \frac{\sqrt{\hat{\epsilon}^*} - \sqrt{\hat{\mu}^*}}{(\sqrt{\hat{\epsilon}^*} + \sqrt{\hat{\mu}^*})^3} \tag{12}$$

and

$$\frac{\partial R^*}{\partial \mu^*} = -2 \frac{\sqrt{\hat{\epsilon}^*}}{\sqrt{\hat{\mu}^*}} \frac{\sqrt{\hat{\epsilon}^*} - \sqrt{\hat{\mu}^*}}{(\sqrt{\hat{\epsilon}^*} + \sqrt{\hat{\mu}^*})^3}. \tag{13}$$

Therefore,

$$\frac{\partial R^*}{\partial \hat{\mu}^*} = -\frac{\hat{\epsilon}^*}{\hat{\mu}^*} \frac{\partial R^*}{\partial \hat{\epsilon}^*}. \tag{14}$$

Substituting this expression into Equation 11 yields the condition for a change in the sign of the derivative

$$\frac{dR^*}{dv_p} = 2 \frac{\sqrt{\hat{\mu}^*}}{\sqrt{\hat{\epsilon}^*}} \frac{\sqrt{\hat{\epsilon}^*} - \sqrt{\hat{\mu}^*}}{(\sqrt{\hat{\epsilon}^*} + \sqrt{\hat{\mu}^*})^3} \left(\frac{\partial \hat{\epsilon}^*}{\partial v_p} - \frac{\hat{\epsilon}^*}{\hat{\mu}^*} \frac{\partial \hat{\mu}^*}{\partial v_p} \right) = 0. \tag{15}$$

Equation 15 indicates that there are two primary cases when nonmonotonicity can occur. The first case is when the relative effective permittivity and relative effective permeability match,

$$\hat{\epsilon}^* = \hat{\mu}^* \Rightarrow \frac{dR^*}{dv_p} = 0. \tag{16}$$

This also implies that the effective reflectance is zero. This can occur if the relative permittivity of the matrix is greater than its relative permeability, $\hat{\epsilon}_m > \hat{\mu}_m$, while the relative permittivity of the particulates is less than their relative permeability, $\hat{\epsilon}_p < \hat{\mu}_p$ or vice versa. To see this, consider starting from $v_p = 0$, with $\hat{\epsilon}_m > \hat{\mu}_m$, $\hat{\epsilon}_p < \hat{\mu}_p$ and increasing the volume fraction until $v_p = 1$ (completely particulate material), one must pass (at least) through one point where $\hat{\epsilon}^* = \hat{\mu}^*$. The second case of nonmonotone condition occurs when

$$\left(\frac{\partial \hat{\epsilon}^*}{\partial v_p} - \frac{\hat{\epsilon}^*}{\hat{\mu}^*}\frac{\partial \hat{\mu}^*}{\partial v_p}\right) = 0 \Rightarrow \frac{dR^*}{dv_p} = 0, \tag{17}$$

which transpires when the ratio of the relative effective permeability to the relative effective permittivity is the same as the ratio of the partial derivative of the relative effective permeability with respect to the volume fraction of second phase particles to the partial derivative of the relative effective permittivity with respect to the volume fraction of second phase particles. In other words,

$$\frac{\hat{\epsilon}^*}{\hat{\mu}^*} = \frac{\frac{\partial \hat{\epsilon}^*}{\partial v_p}}{\frac{\partial \hat{\mu}^*}{\partial v_p}}. \tag{18}$$

For a fixed set of particulate and matrix properties, the conditions in Equation 16 and 18 indicate when the correlation of a specific effective reflectance to a specific volume fraction of particles may not be unique. For example, this information is important when calibrating laboratory tests, such as the mentioned laser velocemitry experiments, or when attempting to determine the level of particulate additives to add to a (binding) matrix to design coatings and paints. Further quantitative investigation of the dependence of the effective reflectance on the microstructure requires numerical simulation, which is actively being pursued.

Acknowledgments: The authors wish to thank Dr. David Walther and Prof. Conrad Stoldt for helpful discussions during the preparation of the this paper. Also, the authors wish to thank DARPA for financial support during this research.

References

1. Bale-Glickman, J., Selby, K., Saloner, D. and Savas, O. 2003. Physiological flow studies in exact-replica atherosclerotic carotid bifurcation. Proceedings of IMECE'03,2003 ASME International Mechanical Engineering Congress and Exposition. Washington, D.C. 16-21.
2. Bale-Glickman, J., Selby, K., Saloner, D. and Savas, O. 2003. Experimental flow studies in exact-replica phantoms of atherosclerotic carotid bifurcations under steady Input conditions, J. Biomech. Eng,125, 38-48.
3. Beckwith, S., Henning, T. & Nakagawa, Y. 2000. Dust Particles in Protoplanetary Disks. *Protostars & Planets IVs*, Mannings, V. & Boss, A.P. & Russell, S.S., editors, University of Arizona Press, Tuscon
4. Benz, W. 2000. From dust to planets. Spatium, 6, pp. 3-14.

5. Blum, J. & Wurm G. 2000. Impact simulations on sticking, restructuring, & fragmentation of preplanetary dust aggregates. Icarus, 143, pp. 138-146.

6. Born, M. & Wolf, E. 2003. *Principles of optics. 7th edition.* Cambridge University Press.

7. Chan, R. C., Chau, A. H., Karl. W. C., Nadkarni, S., Khalil, A. S., Shishkov, M., Tearney, G. J., Kaazempur-Mofrad, M. R., Bouma, B. E. 2004. OCT-based Arterial Elastography: Robust Estimation exploiting Tissue Biomechanics, Optics Express, Vol. 12 19 :4558-4572.

8. Chau, A. H., Chan, R. C., Shishkov, M., MacNeill, B., Iftima, N., Tearney, G. J., Kamm, R. D., Bouma, B., Kaazempur-Mofrad, M.R. 2004. Mechanical Analysis of Atherosclerotic Plaques based on Optical Coherence Tomography, Annals of Biomedical Engineering, 32 11 :1492-1501.

9. Chokshi, A., Tielens, A. G. G. M. & Hollenbach, D. 1993. Dust Coagulation. The Astrophysical Journal. 407, pp. 806-819.

10. Chung, J., Grigoropoulos, C. & Greif, R. 1999. Infrared thermal velocimetry in MEMS-based fluid devices. Journal of Microelectromechanical Systems. Vol. 12, No. 3. pp. 365-371.

11. Cuzzi, C. N., Dobrovolskis, A. R. & Champney, J.M. 1993. Particle-gas dynamics in the midplane of a protoplanetary nebula. *Icarus*, 106, 102-134.

12. Dominik, C. & Tielens, A. G. G. M. 1997. The physics of dust coagulation & the structure of dust aggregates in space. The Astrophysical Journal, 480, pp. 647-673.

13. Khalil, A. S., Chan, R. C., Chau, A. H., Bouma, B. E., Kaazempur-Mofrad, M. R. 2005. Tissue Elasticity Estimation with Optical Coherence Elastography: Toward Mechanical Characterization of In Vivo Soft Tissue, Annals of Biomedical Engineering, 33 11 :1631-1639.

14. Luo, L. and Dornfeld, D. A. 2001. Material removal mechanism in chemical mechanical polishing: theory and modeling. *IEEE Transaction: Semiconductor Manufacturing.* Vol. 14, No. 2, pp.112- 133.

15. Luo, L. and Dornfeld, D. A. 2003. Effects of abrasive size distribution in chemical-mechanical planarization: modeling and verification. *IEEE Transaction: Semiconductor Manufacturing.* Vol. 16, pp. 469-476.

16. Luo, L. and Dornfeld, D. A. 2003. Material removal regions in chemical mechanical planarization for sub-micron integration for sub-micron integrated circuit fabrication: coupling effects of slurry chemicals, abrasive size distribution, and wafer-pad contact area. *IEEE Transaction: Semiconductor Manufacturing.* Vol. 16, pp. 45-56.

17. Luo, L. and Dornfeld, D. A. 2004. Integrated modeling of chemical mechanical planarization of sub-micron IC fabrication. *Springer-Verlag.*

18. Zohdi, T. I. 2004. A computational framework for agglomeration in thermo-chemically reacting granular flows. *Proceedings of the Royal Society.* Vol. 460, 3421-3445.

19. Zohdi, T. I. 2006a. On the optical thickness of disordered particulate media. *Mechanics of Materials.* Volume 38, 969-981.

20. Zohdi, T. I. 2006b. Computation of the coupled thermo-optical scattering properties of random particulate systems. *Computer Methods in Applied Mechanics & Engineering.* Available at: http://www.sciencedirect.com/science/journal/00457825

21. Zohdi, T. I and Kuypers, F. A. 2006. Modeling and rapid simulation of multiple red blood cell light scattering. *Proceedings of the Royal Society Interface.* Volume 3, Number 11 Pages 823-831.

22. Zohdi, T. I. 2007. *Introduction to the modeling and simulation of particulate flows.* SIAM (Society for Industrial and Applied Mathematics).